Rutile to Anatase phase transition induced by N doping in epitaxial TiO_2 films with different dopant distributions

Andrew Breeson[1, 2], Gopinathan Sankar[1], Gregory Goh Kia Liang[2], Robert G. Palgrave*[1]

[1] Department of Chemistry, University College London, 20 Gordon Street, London, UK, WC1E 0AJ

[2] Institute of Materials Research and Engineering, 2 Fusionopolis Way, #08-03 Innovis, Singapore 138634

Abstract

TiO_2 thin films were deposited epitaxially onto Al_2O_3 (0001), $SrTiO_3$ (001), and $LaAlO_3$ (001) single crystal substrates from a titanium alkoxide precursor solution followed by annealing. The films were nitrogen doped by two different routes: either by adding tetramethyethylenediamine (TMEDA) to the precursor solution or alternatively by high temperature ammonolysis. Undoped TiO_2 films were epitaxial and the phase was dependent on the substrate. N doping by ammonolysis led to transformation of rutile films to anatase, confirmed by XRD and by XPS valence band spectroscopy. Similarly, N doping using TMEDA led to stabilisation of anatase films on all substrates. Significant differences were observed in the spatial distribution of the nitrogen dopant depending upon which synthesis method was used. These two factors may shed light on the increased photocatalytic efficiencies reported in N doped TiO_2.

Introduction

Titanium dioxide, TiO_2, is of great importance in modern materials chemistry. It is perhaps the best characterised oxide in terms of defect chemistry,[1] phase transitions,[2] surface structure,[3] surface chemistry,[4] optical properties,[5] and electronic structure.[6] It is of use in a very wide range of current and potential future applications: as the prototypical photocatalyst,[7] as an electron transport layer in solar cells,[8] as a support for heterogeneous catalysts,[9] as a self-cleaning material,[10] as a pigment in paint,[11] and so on. Several polymorphs of TiO_2 are known, including rutile, anatase, brookite and TiO_2(B). The relationship between the anatase and rutile phases, and their relative stability and interconversion, has been particularly well studied. For very small particle sizes, below 10 nm, the anatase phase is more thermodynamically stable.[12] At larger particle sizes, rutile is more thermodynamically stable, and so anatase transforms to rutile at a rate dependent on particle size[12, 13] and presence of impurities.[13, 14] The anatase to rutile transformation is typically rapid at temperatures above 650^{o}C .[2]

TiO_2 was the first material discovered to be photocatalytic,[15] and remains of central importance to the field. The phase composition is especially important for photocatalytic applications. The anatase phase is considered to have higher photocatalytic activity, yet a combination of rutile and anatase together is also a highly effective photocatalyst, due to charge carrier separation across the interface between the phases.[6] It has been recognised that the limiting factor for application of TiO_2 for solar photocatalysis is that the absorption edge is in the near UV range at approximately 380 nm.[15] Much research has been undertaken in an attempt to shift this absorption edge into the visible region of the electromagnetic spectrum in order to use more efficiently the available light. It has been shown that the optical absorption of TiO_2 can be altered by introducing dopants, and it is possible to lower the band gap into the visible region by incorporating a small percentage of nitrogen into the lattice.[16] The exact mechanism via which the catalysis proceeds in tandem with nitrogen still remains uncertain, but if efficient visible light photocatalysis could be achieved with TiO_2 the subsequent beneficial applications would be vast. As an example, self-cleaning surfaces could function inside using indoor lighting and could therefore dramatically improve the sanitation of healthcare environments.[17] Thin films of TiO_2 have proven themselves capable of many photocatalytic oxidations of potentially harmful organisms such as bacteria[18] and viruses,[19] but as yet, a visible light analogue of this has yet to be developed.

There are three prevailing theories for how nitrogen doping of titanium dioxide generates visible light photoactivity. It could be due to substitutional nitrogen doping, or interstitial doping, or nitrogen does not play a role and the real reason is that doping (interstitial or substitutional) promotes the formation of oxygen vacancies.[20, 21] If

the nitrogen doping is substitutional the oxygens in the lattice are directly replaced with nitrogen. However, to balance the charge, an oxygen vacancy must be created for each nitride ion incorporated. Hence substitutional nitrogen doping promotes oxygen vacancies in the lattice.[22]

If the nitrogen doping is interstitial, the oxide ions are not directly replaced. Instead, the nitrogen incorporates itself in some form into the lattice on the interstitial sites with the formation of a Ti-O-N bond.[21] Interstitial doping will occur under mild ammonolysis conditions. The dopants in the interstitial sites also promote the formation of oxygen vacancies. However, the greater the concentration of interstitial doping that occurs, the more oxygen vacancies are created, meaning that an increase in substitutional doping will occur. It is therefore a delicate balance to achieve a sample that is doped in just one way, and most N-TiO_2 samples are a combination of interstitially and substitutionally doped with oxygen vacancies pervading throughout.

Once nitrogen is incorporated into the TiO_2 lattice it can either alter the band structure or suppress how efficiently the electron-hole pairs recombine.[23] It has been shown in anatase titania that if the concentration of nitrogen in the lattice is relatively low then it promotes a large decrease in the formation energy of oxygen vacancies from 4.2 eV to 0.6 eV.[24] The theory of why this occurs is that the excess electrons that are created in the oxygen vacancies get trapped on the nitrogen sites. These oxygen vacancies have been credited with enhancing the photocatalytic activity of TiO_2, however some authors debate as to whether the presence of the oxygen vacancies actually leads to a poorer performance as they act as recombination sites for the electron-hole pairs.[25]

The type of doping that occurs can be deduced via XPS techniques. It is now generally agreed upon that there will be a peak exhibited at approximately 396 eV if the sample has been doped substitutionally, whereas interstitially doped nitrogen exhibits a peak at 400 eV. Often, XPS results show a mixture of these two peaks.

From previous DFT calculations modelling the density of states within N-doped anatase TiO_2,[26] it has been shown that the valance band increased in energy by approximately 0.14 eV when substitutional nitrogen doping occurred. This is due to the mixing of oxygen and nitrogen 2p orbitals. With interstitial N-doping, it has been calculated that a new, narrow band is created approximately 0.74 eV above the valence band.[27]

As has been described above, there has been considerable effort to understand the effect of the microscopic arrangement of N dopants – i.e. whether they are substitutional or interstitial. However, a factor far less commonly investigated is the macroscopic arrangement of the dopants, or the location of the N dopants whether homogeneously distributed throughout the sample, segregated to the surface or to the bulk. It is largely unknown how synthesis and processing methods affect the macroscopic dopant distribution. The physical location of the dopants may play an important role in photocatalysis, not least in affecting the transport of photoexcited charge carriers. To understand how the nitrogen is distributed when incorporated into the TiO_2 lattice will give a clearer indication of how photocatalysis occurs and what role nitrogen plays, as solid state catalysis is dependent on interfaces between compounds. Here we report a study of the nitrogen dopant distribution in epitaxial thin films of anatase and rutile in order to ascertain the effect of synthesis and processing conditions on dopant distribution. We show that smaple processing strongly affects the macroscopic dopant distribution in the materilas studied. Furthermore, we show that in rutile (110) orientated films, the incorporation of nitrogen induces a reverse rutile-to-anatase phase transition at high temperature, which we believe has not been observed previously. This reverse phase transition occurs through two different methods of N doping, and may explain some of the enhanced photoactivity seen in N doped materials by phase transformation rather than direct visible light absorption.

Experimental Section

Single crystal substrates: Al_2O_3 (0001), $SrTiO_3$ (001) and $LaAlO_3$ (001) were purchased from PI-KEM Ltd. Substrates were 10x10x1 mm^3 in size and were epi-polished on both sides by the manufacturer. Prior to use, substrates were cleaned by ultrasonication in acetone followed by isopropanol, and were dried under a stream of nitrogen gas.

The solution phase route to TiO_2 films is adapted from Powell *et al.*[28] Acetylacetone (0.025 mol: 2.52 g) was added to butan-1-ol (32 cm^3), followed by addition of titanium *n*-butoxide (0.05 mol: 17.50 g) and left to stir vigorously for 1 hour at room temperature. Isopropanol (0.15 mol: 9.05 g) dissolved in distilled water (3.64 cm^3) was

added and the solution left to stir for 1 hour at room temperature. Finally acetonitrile (0.04 mol: 1.66 g) was added and the solution was left to stir for a further 1 hour at room temperature.

This solution was used to deposit nominally undoped TiO_2 films. To deposit nitrogen doped films, tetramethylethylenediamine (TMEDA, 0.0129 mol: 1.5g) was added to the sol and left to stir for 1 hour at room temperature. In both cases (undoped TiO_2 sol or N doped TiO_2 sol) the solution was then sealed and left overnight to age.

After aging, the solution was deposited onto the desired single crystal substrate via dynamic dispense at 1000 rpm, then spun at 3000 rpm for 30 seconds. These depositions steps were repeated 5 times without interlayer annealing for each film. After deposition, the thin film samples were annealed in air at 800 °C for 2 hours to effect crystallisation. For post-annealing nitrogen doping, nominally undoped TiO_2 epitaxial thin films on single crystal substrates were heated in a tube furnace under ammonolysis conditions (675 °C, flowing anhydrous ammonia gas) for 3 hours. The flow rate of the ammonia was 600 sccm and the samples were heated up and down under flowing nitrogen with a ramp rate of 10 °C / minute. Once cooled to room temperature, samples were handled and stored in air.

Results

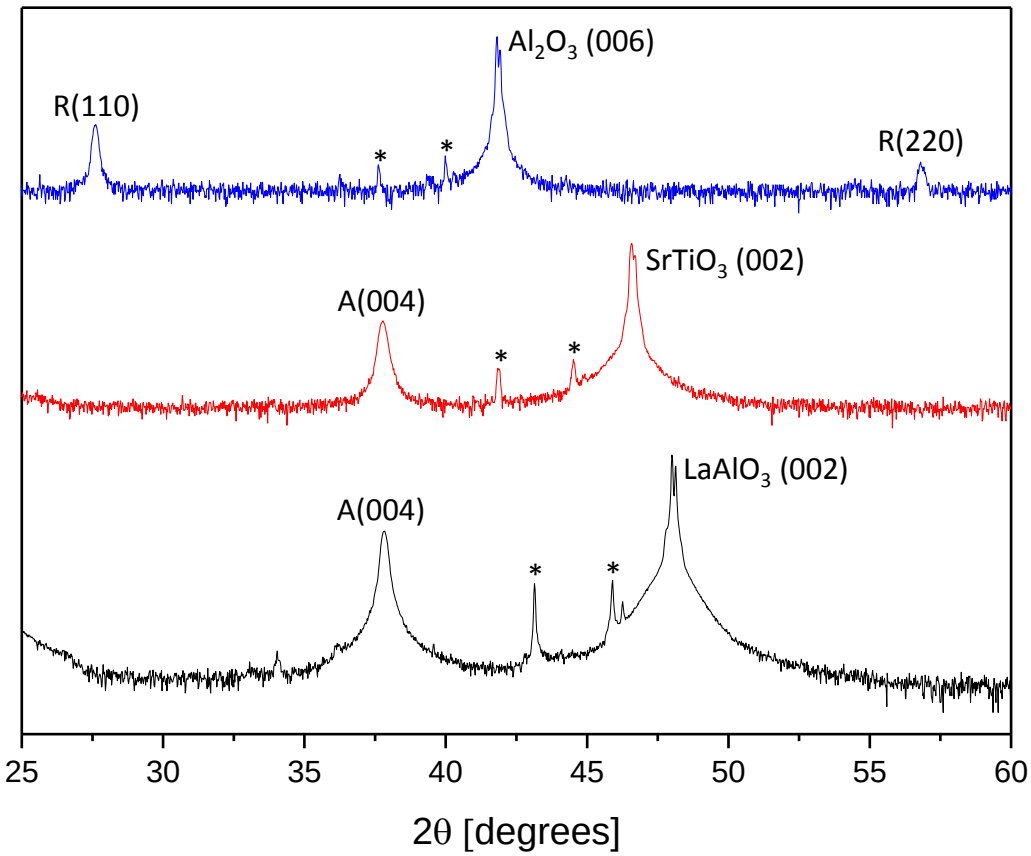

Figure 1. XRD of epitaxial rutile (110) and (220) TiO_2 grown on Al_2O_3 (0001) and anatase (004) TiO_2 grown on $SrTiO_3$ (001) and $LaAlO_3$ (001). The intensity ordinate is on a log scale, with separate scans offset for clarity. Peaks marked with an asterisk originate from the substrate and are an instrumental artefact due to additional wavelengths present in the X-ray radiation.

Epitaxial films of undoped TiO_2 were produced on Al_2O_3 (0001), $SrTiO_3$ (STO) (001), and $LaAlO_3$ (LAO) (001) oriented substrates (Fig. 1). The perovskite structured substrates STO and LAO were found to template a-TiO_2 as observed by others.[29-31] Films grown on STO and LAO showed only one diffraction peak from the film, assigned as a-TiO_2 (004), consistent with (001) orientated growth of the anatase phase. The peaks originating from the single crystal substrates were used as internal references to calibrate the 2θ range for calculation of the thin film lattice parameters. The a-TiO_2 (004) peak from the film grown on LAO was measured at 2θ=37.90°, giving d_{004} = 2.374 Å

corresponding to c = 9.496 Å, very close to the c parameter expected in bulk a-TiO_2 of 9.515 Å. The coincidence of the epitaxial film out-of-plane lattice parameter with the bulk lattice parameter indicates that there is little epitaxial strain in this film. For a-TiO_2 films deposited on STO, the a-TiO2 (004) diffraction peak appeared at 2θ=37.64° giving d_{004} = 2.390 Å corresponding to c = 9.560 Å, slightly larger than the bulk parameter. This is unexpected, as previously a-TiO_2 films on STO (001) have shown slightly reduced *c* parameters compared to the bulk, due to tensile strain.[32]

Growth of TiO_2 on Al_2O_3 (0001) crystals was found to template r-TiO_2 growth; only the r-TiO_2 (110) and (220) diffraction peaks were present in the angular range measured, indicating a (110) orientation of the deposited film. The r-TiO_2 (110) peak appeared at 2θ=27.47°, giving d_{110} = 3.247 Å corresponding to a = 4.592 Å, matching the reported bulk r-TiO_2 lattice parameter of a = 4.594 Å. Thus the rutile phase appears unstrained, although the absence of any other r-TiO_2 peaks indicates that the film is templated by the substrate; for example the r-TiO_2 (211) peak, expected at 2θ=54.4° with intensity 51% of the (110) peak, is absent in the XRD pattern from the film. The stabilisation of the r-TiO_2 (110) orientation by Al_2O_3 (0001) is unexpected, however. Several studies of TiO_2 grown using physical vapour deposition techniques report rutile (001) being produced epitaxially on Al_2O_3 (0001),[33-36] to the best of our knowledge this is the first reported case of epitaxial r-TiO_2 (110) on this Al_2O_3 surface.

X-ray photoelectron spectroscopy of the TiO_2 films on different substrates confirmed the expected surface composition of Ti, O and carbon contamination. Valence band (VB) scans were carried out and are shown in Fig. 2. The VB spectrum of r-TiO_2 and a-TiO_2 have distinctive shapes, where VB spectra from commercial powders of each phase are shown. Both phases consist of a VB spectrum with two distinct maxima separated in binding energy by approximately 2.5 eV. However, in r-TiO_2, the two maxima are approximately equal in height, whereas in a-TiO_2 the larger binding energy maximum is considerably greater in height. Thus these two polymorphs of TiO_2 can be distinguished by comparing the VB spectra. The VB spectra from the epitaxial films on LAO, STO and Al_2O_3 can be seen to follow the expected pattern. The films on LAO and STO have VB spectra closely resembling the a-TiO_2 standard, whilst the film on Al_2O_3 has a VB spectrum closely resembling r-TiO_2. This supports the XRD analysis, and further confirms that the surface of these materials has the same crystal structure as the bulk.

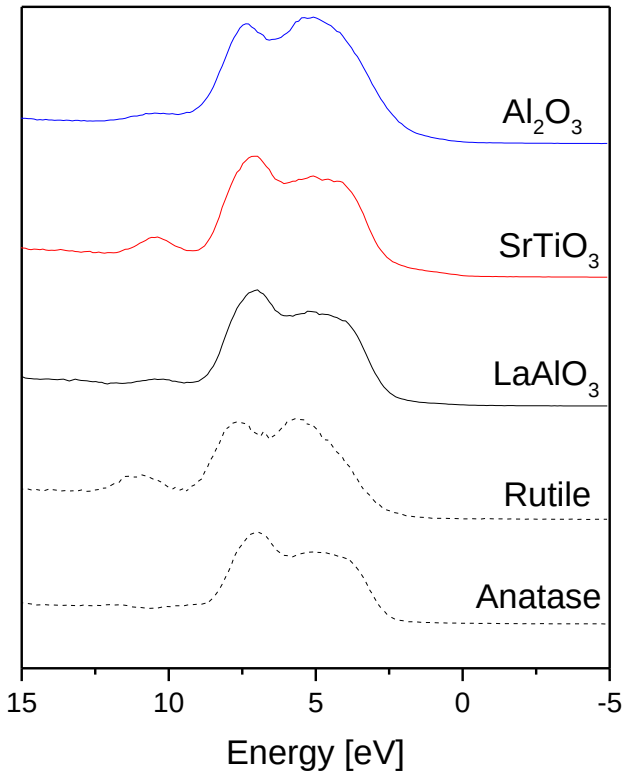

Figure 2. Valence band spectrum of epitaxial rutile (110) TiO_2 films grown on Al_2O_3 (0001) and anatase (004) TiO_2 grown on $SrTiO_3$ (001) and $LaAlO_3$ (001) compared with the standard valance bands of rutile and anatase.

Nitrogen doping by ammonolysis

After deposition, each epitaxial TiO_2 film described in the previous section was heated under flowing ammonia at 1 sccm at 675°C for 1.5 and 3.0 hours to induce N doping. XRD showed the epitaxial nature of the anatase films on STO and LAO remained unchanged, with lattice parameters identical before and after ammonolysis. After exposure to these ammonolysis conditions for 1.5 hours, the r-TiO_2 film on Al_2O_3 (0001) also showed unchanged XRD patterns (Fig. 3). However, after 3 hours the diffraction peaks corresponding to a-TiO_2 emerged at 2θ=25.30° and 2θ=48.05° corresponding to a-TiO_2 (101) and (200) reflections respectively. There are examples of nitrogen doping TiO_2 promoting anatase formation or raising the anatase to rutile transition temperature, [37-39] but to our knowledge no previous report of interconversion of rutile to anatase at high temperature exists.

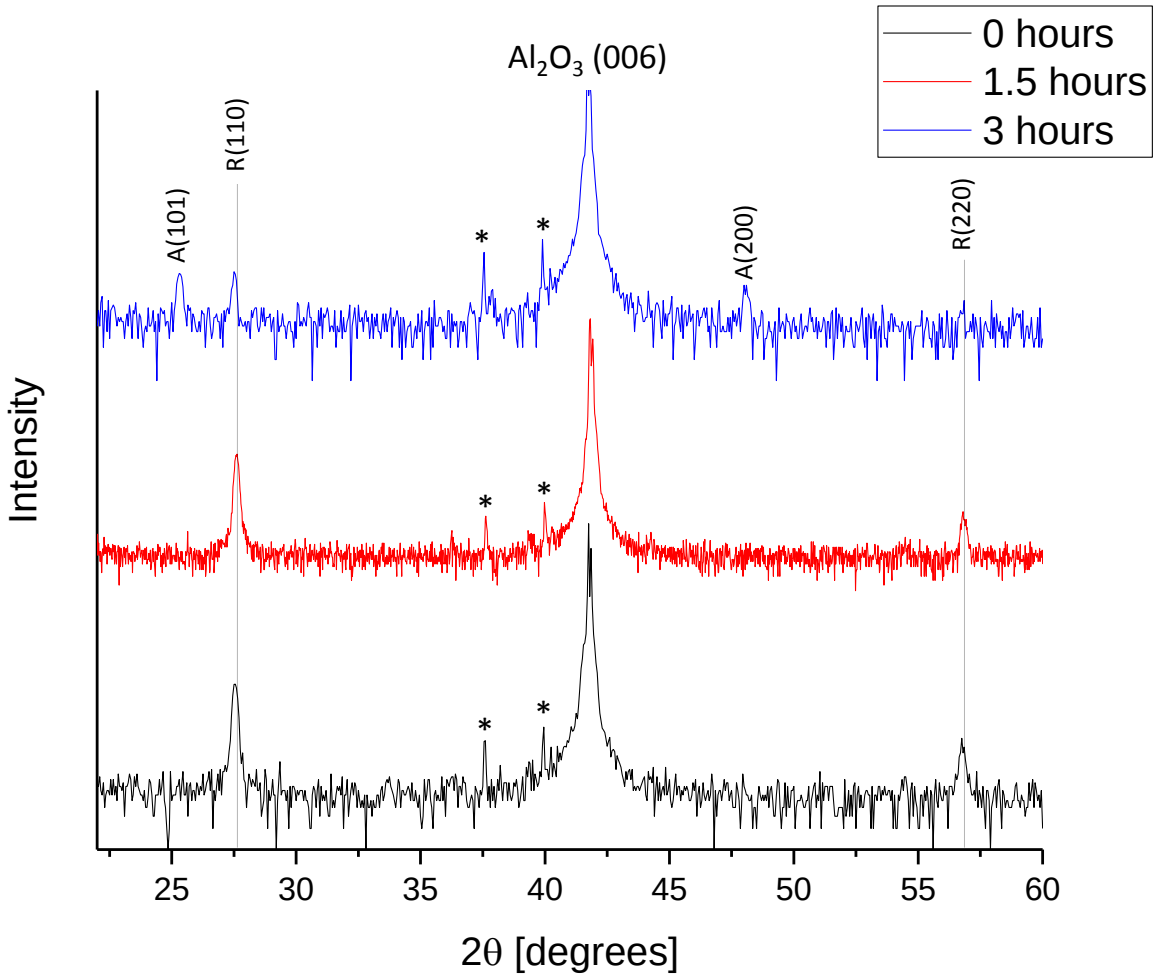

Figure 3. XRD of epitaxial rutile (110) and (220) TiO_2 grown on Al_2O_3 (0001). After 1.5 hours of N doping there is no change. After 3 hours there has been a rutile to anatase conversion. Peaks marked with asterisks originate from the substrate and are an instrumental artefact due to additional wavelengths present in the X-ray radiation.

To further study this interconversion, the XPS valence bands were measured. Fig. 4 shows a comparison between the valence bands of the pure and doped epitaxial films. Care must be taken as it is known that nitrogen doping itself can cause changes to the valence band of TiO_2 (for both substitutional and interstitial doping), [40-44] especially introduction of spectral intensity within the band gap (at the low binding energy side of the valence band spectrum), either as localised states close to the Fermi level due to reduction of Ti and filling of the Ti 3d level, or a tailing of the valence band edge due to incorporation of N 2p states. However, both of these changes tend to be relatively minor compared with the differences between rutile and anatase valence band structures already discussed. Therefore we propose that the valence band shape can still be used to differentiate anatase and rutile in these N doped systems. It is clear that a change occurs in the appearance of the VB spectrum in the r-TiO_2 film deposited on Al_2O_3 after ammonolysis. Whereas before N doping, the VB spectrum resembled that of a standard sample of r-TiO_2, after 1.5 hours of ammonolysis the relative heights of the VB maxima have changed, and by 3 hours of ammonolysis the VB resembles closely that of a-TiO2 standard. That the XPS valence band begins to change in

shape (after 1.5 hours) before a change in crystal structure can be detected in XRD suggests that the phase transformation begins at the surface of the material (as XPS is highly surface sensitive). This is consistent with the rutile to anatase phase transformation being caused by incorporation of nitrogen from the ammonolysis process.

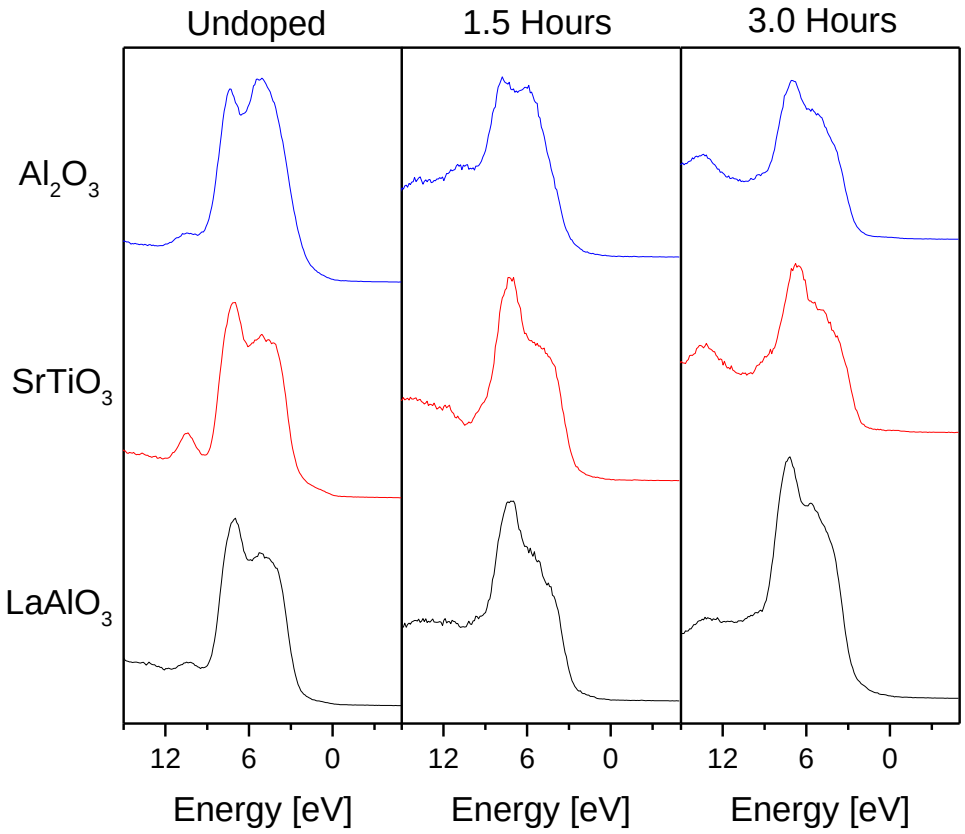

Figure 4. A comparison of the valence bands of pure TiO_2 epitaxial thin films and TiO_2 doped via the ammonolysis method

Fig. 5 shows the N 1s XP spectra from the epitaxial films as presented after 3 hours of ammonolysis treatment. The binding energy scale was calibrated to adventitious C 1s at 284.8 eV. All films exhibit N 1s peaks at a binding energy between 395-7 eV, which has been assigned to substitutional nitride anions on oxide sites within TiO_2. In all cases there is also a broader, higher binding energy peak centred between 398-400 eV. This environment is associated with interstitially doped nitrogen. There is no indication of a peak above 400 eV in any sample: peaks above 400 eV correspond to oxidised nitrogen species such as nitrates.

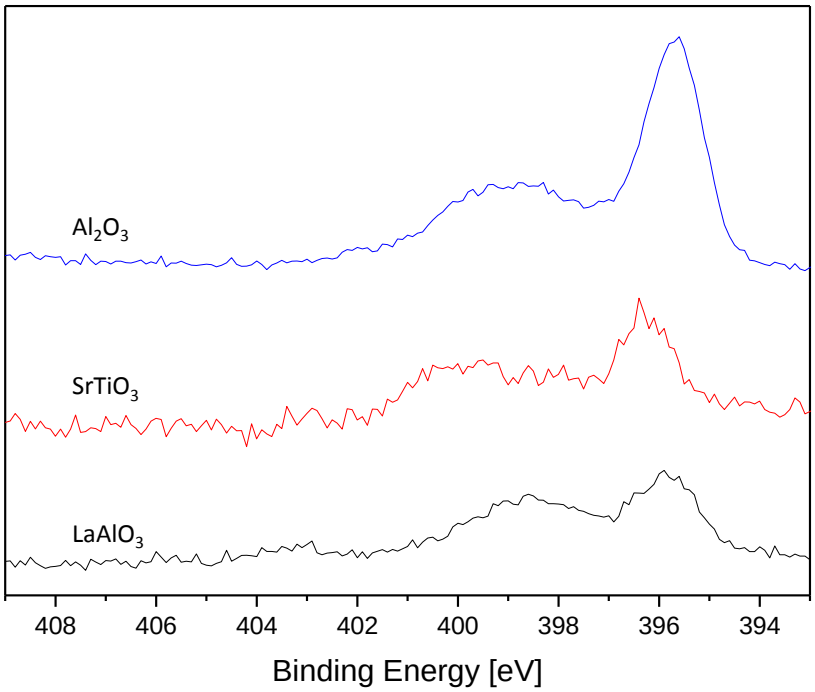

Figure 5. Photoemission spectra of the N 1s core lines in the films of epitaxial TiO_2 on various substrates doped via ammonolysis. Intensities of peaks are concordant with depth profile results (Fig. 6).

The films were sputtered in-situ with a monoatomic Ar ion gun to determine the distribution of the N within the films after 3 hours doping. Fig. 6 shows the depth profile of nitrogen incorporated into the thin films as a percentage. All films show a maximum N level at the surface which decreases with etching.

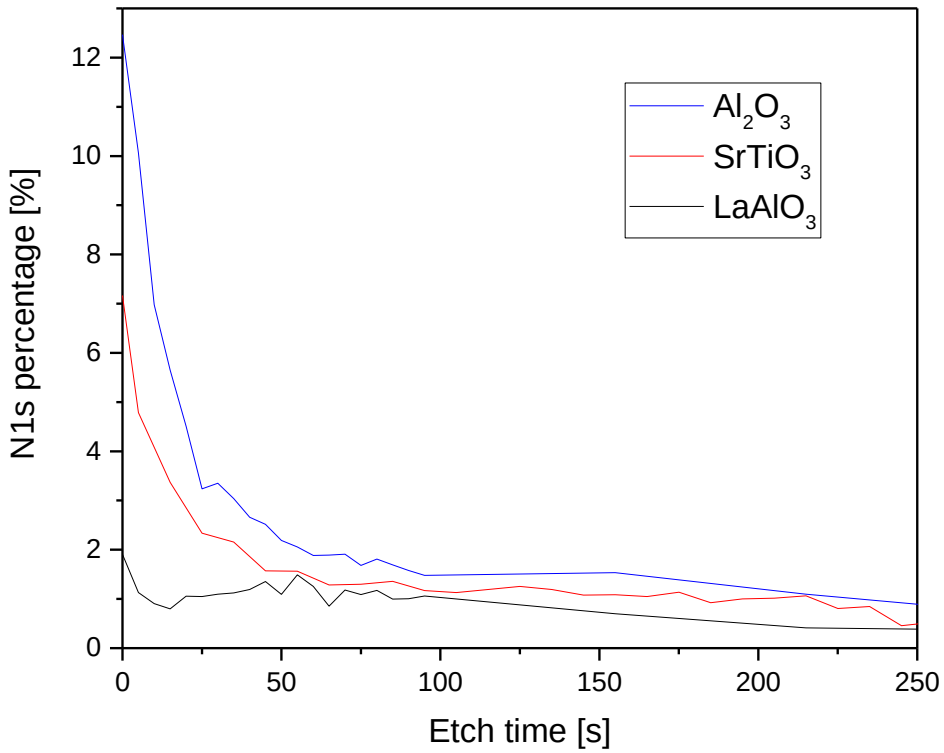

Figure 6. XPS depth profile of N-TiO_2 thin films doped via ammonolysis on differing substrates (Al_2O_3, $SrTiO_3$, $LaAlO_3$).

The film epitaxially produced on the Al_2O_3 substrate showed the highest level of surface nitrogen with a value of 12 % calculated from the scanned elements O, N, C, and Ti. The film on STO showed 7% N after

ammonolysis, whilst the film on LAO showed only 2% N. It is surprising that such a large difference is seen in N doping levels between the two anatase films, on STO and LAO. This may be due to differing surface morphologies which were not measured, or by the difference in strain: the larger strain in the STO supported film may lead to greater N incorporation.

Nitrogen doping using tetramethyethylenediamine (TMEDA)

A second doping method was investigated. N doped TiO_2 films were deposited in a single step by adding TMEDA (0.0129 mol, 1.5g) to the TiO_2 sol prior to coating onto the STO, LAO, and Al_2O_3 single crystal substrates. XRD showed that the presence of the TMEDA did not affect the crystallisation of the films produced on the STO and LAO single crystal substrates which were still oriented with a-TiO_2 (001) as in the undoped films. The film on LAO showed a c-parameter of 9.546 Å, somewhat larger than the undoped LAO film (c = 9.522 Å). In contrast the N doped a-TiO2 film on STO showed a c parameter almost identical to the undoped counterpart.

However, the crystallisation of the film produced on Al_2O_3 (0001) was dramatically affected by the presence of TMEDA. Fig. 7 shows a comparison between the undoped epitaxial rutile film and the two N doping strategies. It can be seen that doping with the nitrogen source in the sol results in a film showing a-TiO_2 (101) and (200) peaks, and only a very weak r-TiO_2 (110) peak. The film can thus be described as a polycrystalline anatase film which grows despite the rutile templating effect of Al_2O_3 (0001) seen in the undoped materials.

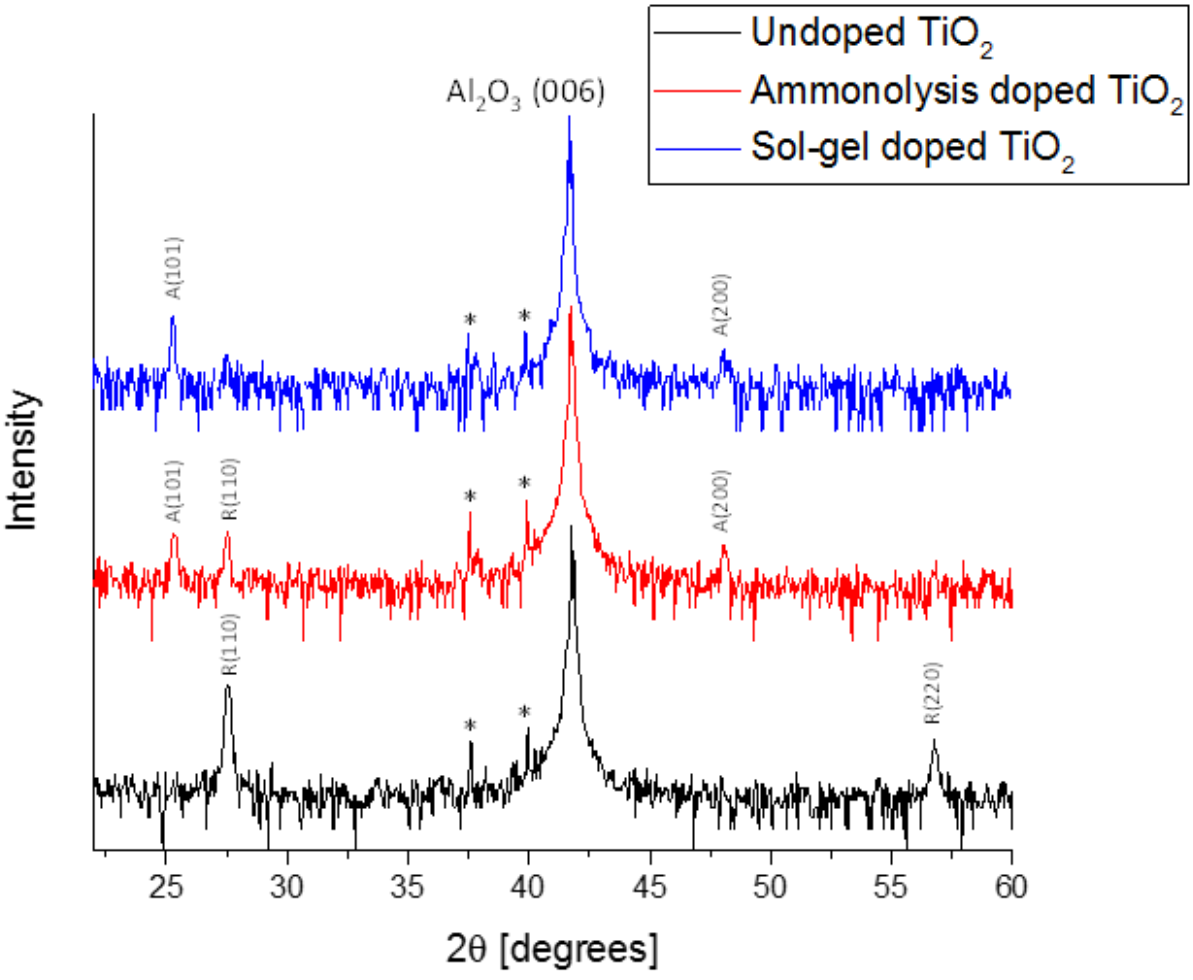

Figure 7. An XRD comparison between the undoped epitaxial r-TiO_2 (110) film and the two N doping strategies. The intensity is on a log scale and offset for clarity.

XPS of the surface nitrogen for the unannealed films in Fig. 8 shows a binding energy of 400-401 eV corresponding to interstitially doped N in the TiO_2 lattice. There is also the presence of a peak at approximately 403 eV which does not tally with interstitially or substitutionally doped N 1s. This peak is indicative of the unreacted dopant left on the surface of the film. Further evidence for this being unreacted dopant is that after annealing it disappears. Fig. 9 shows the annealed films to have an N 1s binding energy of approximately 399-402 eV. Again, this

is evidence for nitrogen being interstitially doped in the TiO_2 lattice, or possibly oxides of nitrogen at the higher end of the binding energy range observed.

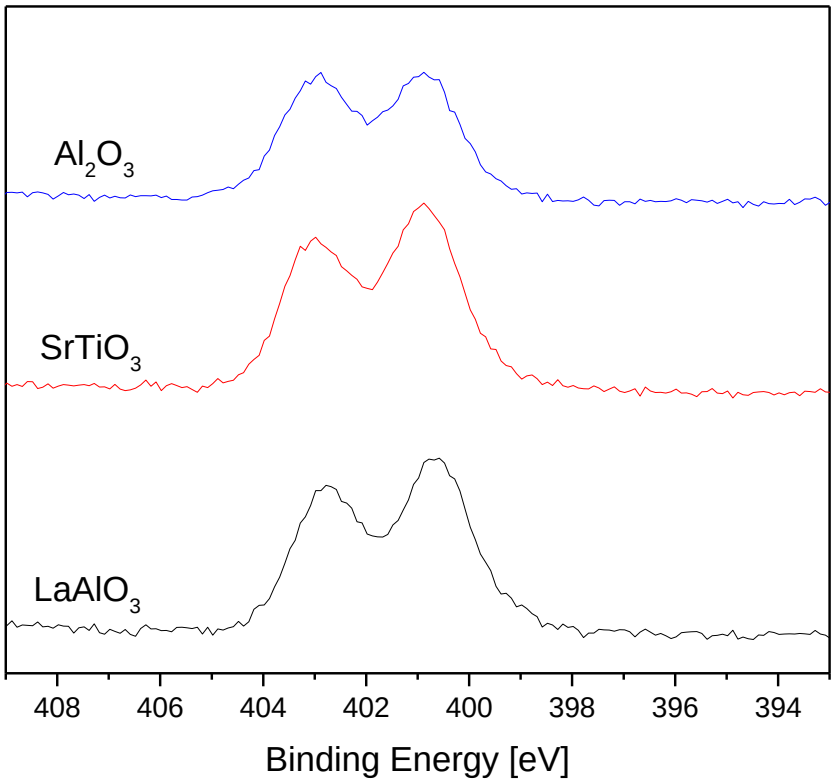

Figure 8. Spectra of the binding energies of N 1s in the unannealed films of TiO_2 doped via TMEDA in the TiO_2 sol.

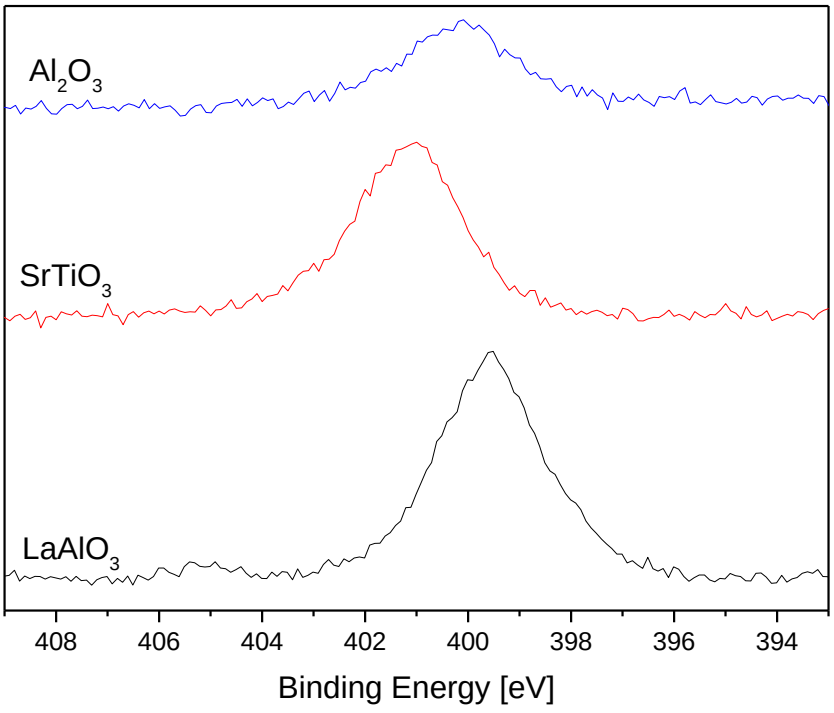

Figure 9. Spectra of the binding energies of N 1s in the annealed films of TiO_2 doped via TMEDA in the TiO_2 sol.

In Fig. 10, XPS depth profile analysis of the films before and after annealing shows that for all substrates the nitrogen was initially distributed evenly throughout, although the surface appeared nitrogen depleted compared with the bulk. Upon annealing however, the nitrogen distribution shows a heavy migration to the films surface. Despite being concentrated at the surface post annealing, there is still trace amounts of nitrogen throughout the films. Calculating the area under the two differing curves shows an approximate loss of 90 %, 88 %, and 84 % nitrogen within the depth measured for Al_2O_3, STO, and LAO films respectively. This migration and loss of nitrogen dopant may be an important process in nitrogen doping of TiO_2 that is likely to impact on the functionality.

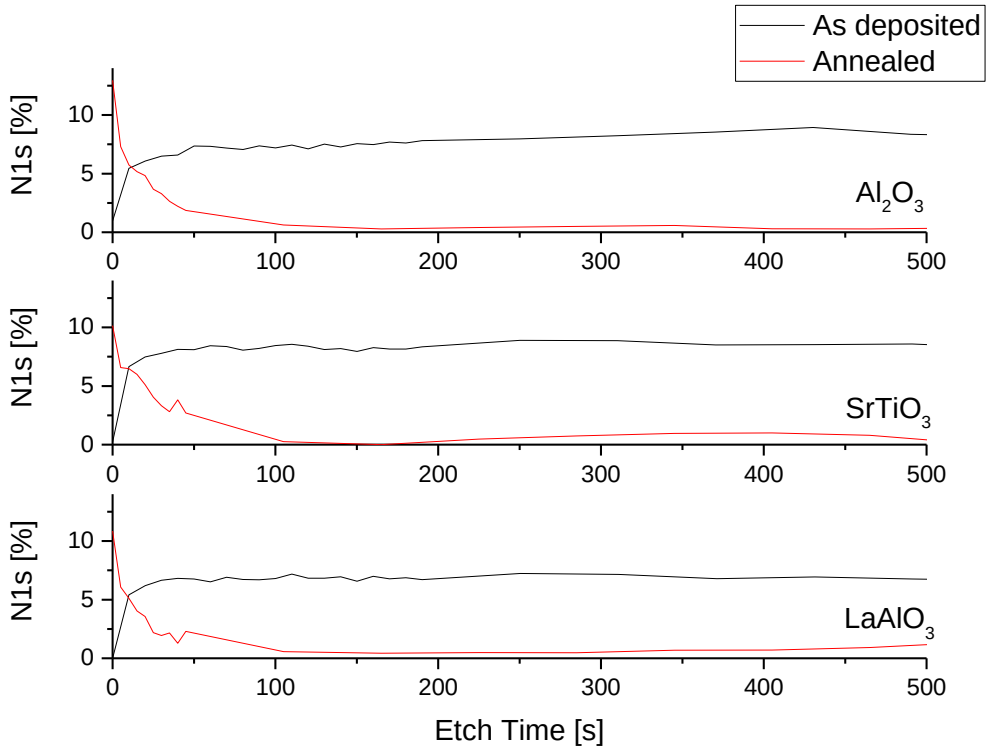

Figure 10. XPS sol-doped depth profiles of N 1s before and after annealing

Figure 11 shows a comparison of the XPS valence bands of the films produced on the varying substrates and their sol-doped counterparts both as-deposited and annealed. As discussed previously, in the undoped epitaxial films the valence band spectra closely resemble the model compounds (a-TiO_2 and r-TiO_2) according to the templating substrate. TMEDA doped samples before annealing show a broad and featureless valence band spectra which can be expected to include contributions from the molecular nitrogen precursor and titanium alkoxide gel film. Post annealing, all samples show valance band spectra that closely resemble the a-TiO_2 standard. This confirms the phase assignment by XRD, and further supports the hypothesis that nitrogen doping stabilises anatase over rutile in these epitaxial systems.

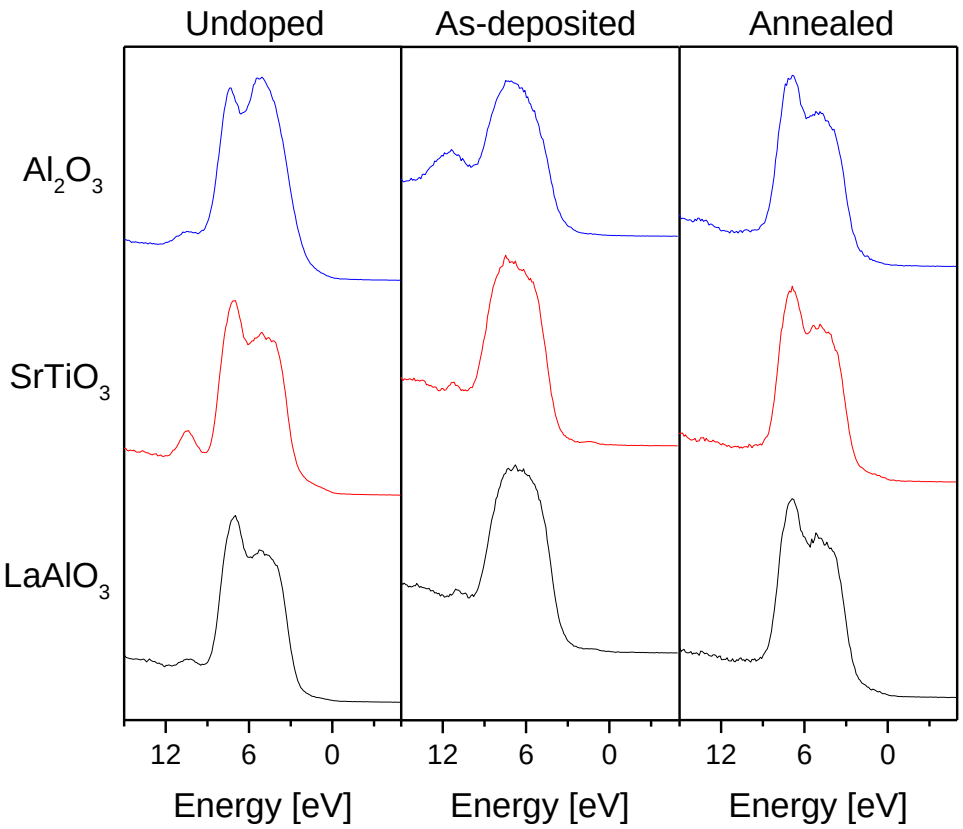

Figure 11. A comparison of the valence bands of thin films of pure TiO_2 (left) and TiO_2 doped via TMEDA in the sol (middle – with no heat treatment and right – after heat treatment to effect crystallisation).

Conclusion

We have studied a series of epitaxial TiO_2 films grown by solution phase methods on perovskite and c-cut sapphire substrates. In accordance with literature precedent, the perovskite substrates templated anatase (001) growth, while the Al_2O_3 (0001) templated rutile. We have studied nitrogen doping through two routes: firstly doping through ammonolysis of the TiO_2 epitaxial films. Secondly, incorporation of a nitrogen precursor into the wet chemical deposition. We report that ammonolysis causes a reverse rutile-to-anatase phase transition in films deposited on Al_2O_3 (0001), and this is confirmed by XRD and valence band XPS, which is used here to distinguish anatase and rutile TiO_2 phases through their differing spectra shapes. Doping with TMEDA also stabilised anatase, and such films showed anatase phase even on the Al_2O_3 (0001) substrate. Depth profiling showed a significant migration of nitrogen from bulk to surface on annealing of TMEDA doped TiO_2 epitaxial films.

These results shed light on previously unknown aspects of the N doping process in TiO_2. The rutile to anatase transition seen here may help explain the enhanced photocatalytic performance of N doped TiO_2, as rutile-anatase heterojunctions are known to be highly effective at promoting photocatalysis.

References

1. M. K. Nowotny, L. R. Sheppard, T. Bak and J. Nowotny, *Journal of Physical Chemistry C*, 2008, **112**, 5275-5300.
2. A. W. Czanderna, C. N. R. Rao and J. M. Honig, *Transactions of the Faraday Society*, 1958, **54**, 1069-1073.
3. U. Diebold, *Surface Science Reports*, 2003, **48**, 53-229.
4. M. A. Henderson, *Surface Science Reports*, 2011, **66**, 185-297.
5. S. D. Mo and W. Y. Ching, *Physical Review B*, 1995, **51**, 13023-13032.

6. D. O. Scanlon, C. W. Dunnill, J. Buckeridge, S. A. Shevlin, A. J. Logsdail, S. M. Woodley, C. R. A. Catlow, M. J. Powell, R. G. Palgrave, I. P. Parkin, G. W. Watson, T. W. Keal, P. Sherwood, A. Walsh and A. A. Sokol, *Nature Materials*, 2013, **12**, 798-801.
7. A. Mills and S. LeHunte, *Journal of Photochemistry and Photobiology a-Chemistry*, 1997, **108**, 1-35.
8. B. Oregan and M. Gratzel, *Nature*, 1991, **353**, 737-740.
9. M. S. Chen and D. W. Goodman, *Science*, 2004, **306**, 252-255.
10. I. P. Parkin and R. G. Palgrave, *Journal of Materials Chemistry*, 2005, **15**, 1689-1695.
11. J. H. Braun, A. Baidins and R. E. Marganski, *Progress in Organic Coatings*, 1992, **20**, 105-138.
12. A. A. Gribb and J. F. Banfield, *American Mineralogist*, 1997, **82**, 717-728.
13. K. Okada, N. Yamamoto, Y. Kameshima, A. Yasumori and K. J. D. MacKenzie, *Journal of the American Ceramic Society*, 2001, **84**, 1591-1596.
14. J. Arbiol, J. Cerda, G. Dezanneau, A. Cirera, F. Peiro, A. Cornet and J. R. Morante, *Journal of Applied Physics*, 2002, **92**, 853-861.
15. A. Fujishima and K. Honda, *Nature*, 1972, **238**, 37-+.
16. R. Asahi, T. Morikawa, T. Ohwaki, K. Aoki and Y. Taga, *Science*, 2001, **293**, 269-271.
17. C. W. H. Dunnill, Z. A. Aiken, J. Pratten, M. Wilson, D. J. Morgan and I. P. Parkin, *Journal of Photochemistry and Photobiology a-Chemistry*, 2009, **207**, 244-253.
18. K. Page, R. G. Palgrave, I. P. Parkin, M. Wilson, S. L. P. Savin and A. V. Chadwick, *Journal of Materials Chemistry*, 2007, **17**, 95-104.
19. H. A. Foster, I. B. Ditta, S. Varghese and A. Steele, *Applied Microbiology and Biotechnology*, 2011, **90**, 1847-1868.
20. I. Nakamura, N. Negishi, S. Kutsuna, T. Ihara, S. Sugihara and E. Takeuchi, *Journal of Molecular Catalysis a-Chemical*, 2000, **161**, 205-212.
21. C. W. Dunnill and I. P. Parkin, *Dalton Transactions*, 2011, **40**, 1635-1640.
22. R. Beranek and H. Kisch, *Electrochemistry Communications*, 2007, **9**, 761-766.
23. L. Zhao, Q. Jiang and J. Lian, *Applied Surface Science*, 2008, **254**, 4620-4625.
24. K. Prabakar, T. Takahashi, T. Nezuka, K. Takahashi, T. Nakashima, Y. Kubota and A. Fujishima, *Journal of Vacuum Science & Technology A*, 2007, **25**, 1188-1192.
25. C. Di Valentin, G. Pacchioni, A. Selloni, S. Livraghi and E. Giamello, *Journal of Physical Chemistry B*, 2005, **109**, 11414-11419.
26. Z. Zongyan and L. Qingju, *Journal of Physics D: Applied Physics*, 2008, **41**, 085417.
27. E. Kowalska, O. O. P. Mahaney, R. Abe and B. Ohtani, *Physical Chemistry Chemical Physics*, 2010, **12**, 2344-2355.
28. M. J. Powell, C. W. Dunnill and I. P. Parkin, *Journal of Photochemistry and Photobiology a-Chemistry*, 2014, **281**, 27-34.
29. G. S. Herman and Y. Gao, *Thin Solid Films*, 2001, **397**, 157-161.
30. A. Ito, T. Sato and T. Goto, *Thin Solid Films*, 2014, **551**, 37-41.
31. M. Murakami, Y. Matsumoto, K. Nakajima, T. Makino, Y. Segawa, T. Chikyow, P. Ahmet, M. Kawasaki and H. Koinuma, *Applied Physics Letters*, 2001, **78**, 2664-2666.
32. C. K. Ong and S. J. Wang, *Applied Surface Science*, 2001, **185**, 47-51.
33. N. Sbaï, J. Perrière, W. Seiler and E. Millon, *Surf Sci*, 2007, **601**, 5649-5658.
34. S.-i. Kitazawa, Y. Choi, S. Yamamoto and T. Yamaki, *Thin Solid Films*, 2006, **515**, 1901-1904.
35. T. Roch, E. Dobročka, M. Mikula, A. Pidík, P. Durina, A. A. Haidry, T. Plecenik, M. Truchlý, B. Grancic, A. Plecenik and P. Kúš, *Journal of Crystal Growth*, 2012, **338**, 118-124.
36. S. Yamamoto, T. Sumita, Sugiharuto, A. Miyashita and H. Naramoto, *Thin Solid Films*, 2001, **401**, 88-93.
37. I. Ruzybayev and S. I. Shah, *Surface and Coatings Technology*, 2014, **241**, 148-153.
38. T. Lindgren, J. M. Mwabora, E. Avendaño, J. Jonsson, A. Hoel, C.-G. Granqvist and S.-E. Lindquist, *The Journal of Physical Chemistry B*, 2003, **107**, 5709-5716.
39. F. Kazunori and Y. Isao, *Japanese Journal of Applied Physics*, 1996, **35**, 5790.
40. Y. Cong, J. Zhang, F. Chen and M. Anpo, *Journal of Physical Chemistry C*, 2007, **111**, 6976-6982.
41. S. Livraghi, M. C. Paganini, E. Giamello, A. Selloni, C. Di Valentin and G. Pacchioni, *Journal of the American Chemical Society*, 2006, **128**, 15666-15671.
42. S. Sakthivel, M. Janczarek and H. Kisch, *Journal of Physical Chemistry B*, 2004, **108**, 19384-19387.
43. M. Sathish, B. Viswanathan, R. P. Viswanath and C. S. Gopinath, *Chemistry of Materials*, 2005, **17**, 6349-6353.
44. I. Takahashi, D. J. Payne, R. G. Palgrave and R. G. Egdell, *Chemical Physics Letters*, 2008, **454**, 314-317.